NANO LETTERS

LETTER

pubs.acs.org/NanoLett

Opto-Mechanical Force Mapping of Deep Subwavelength Plasmonic Modes

John Kohoutek, Dibyendu Dey, Alireza Bonakdar, Ryan Gelfand, Alejandro Sklar, Omer Gokalp Memis, and Hooman Mohseni*

Bio-Inspired Sensors and Optoelectronics Laboratory (BISOL), EECS, Northwestern University 2145 Sheridan Road, Evanston, Illinois 60208, United States

Supporting Information

ABSTRACT: We present spatial mapping of optical force generated near the hot spot of a metal−dielectric−metal bowtie nanoantenna at a wavelength of 1550 nm. Maxwell's stress tensor method has been used to simulate the optical force and it agrees well with the experimental data. This method could potentially produce field intensity and optical force mapping simultaneously with a high spatial resolution. Detailed mapping of the optical force is crucial for understanding and designing plasmonic-based optical trapping for emerging applications such as chip-scale biosensing and optomechanical switching.

KEYWORDS: Optical force, NSOM, surface plasmon resonance, AFM, atomic force microscope, biosensing

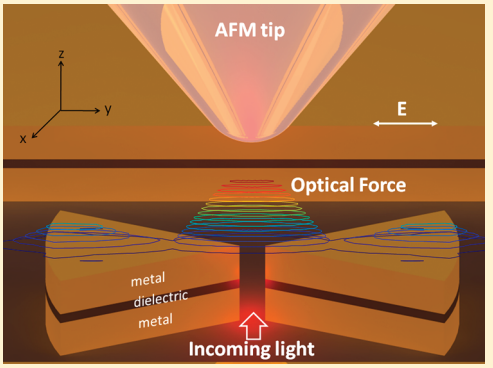

Photons have a momentum (h/λ) and transfer of this momentum to other objects due to elastic scattering is the physical origin of radiation pressure and optical force. This has been known to exist since deduced by Maxwell in 1871, and has been explored in many applications[1] such as solar sails for space propulsion,[2] and more recently radiation cooling.[3,4] However, the force caused by unfocused light is very small, such that for an application such as a solar sail a huge area is needed.[2] Previous work has shown that if the light is focused by traditional lens optics, a force large enough to measure with a probe particle is possible and called optical trapping.[5] This phenomenon has been well developed by the far-field optics community.[6−8] Developmental work has been done with a probe particle held by an optical trap in 2006 to map the force induced by surface plasmon radiation.[9] Recently there has been a lot of interest to exploit the near-field region to generate an optical force to similarly trap particles.[10−12] Near-field trapping was demonstrated by Righini et al. in 2007[13] and has more recently been used to trap even smaller particles.[14] Here, one uses a nanoantenna to focus the light, instead of a lens, and the light can be focused past the diffraction limit using an integrated source. Once the light is focused to this point, a local force in the piconewton range may be expected, as shown by simulation so far.[10−12,15] Furthermore, one can then use the local trapping forces toward building a biosensor utilizing surface plasmon resonance.[16,17] Similar structures have been used for sensing.[18] In fact, in a microfluidic setup, the optical force could be used to enhance the attraction of small particles, and therefore molecules, to the hotspot beyond the diffusion rate.[13,14,16,17] Also, unlike the usual trapping methods, plasmonic nanostructures are ideal for "chip-scale" optical trapping. Most importantly, this allows trapping in volumes that are many orders of magnitude smaller than what could be achieved with far-field optical trapping.[18−20] So far, experimental work done to map optical forces in the near and far-fields have used large probe particles at the expense of high spatial resolution.[5,9] There has been little experimental work in measuring the optical force in the near-field with a high spatial resolution. Following our recent work on measurement of Casimir force with nanometer resolution,[21] here we present an experimental method to accurately map the near-field optical force.

A plasmonic nanoantenna can be used to focus light down to a spot orders of magnitude smaller than the incoming incident wavelength.[19,20,22] These antennas work based on the principle of surface plasmon resonance, a collective oscillation of electrons at the interface between metal and dielectric. Because the optical force originates from the divergence of the electromagnetic energy density,[23] the fact that plasmonics can be used to concentrate the electric field to a very small spot can lead to a very large force density. On the basis of our simulation and experimental analysis,[19,20] we have chosen a metal−dielectric−metal (MDM) bowtie antenna design due to its capability to generate higher near-field enhancement. Such strong optical confinement results in a significant enhancement in electromagnetic field strength and its gradient within this region. Thus, near this "hot spot" region, an optical force up to

Received: May 25, 2011
Revised: July 14, 2011
Published: July 19, 2011

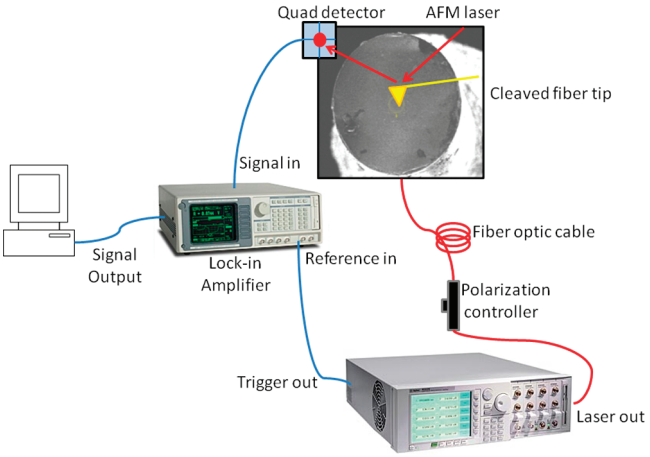

Figure 1. Experimental setup for measuring optical force. The antenna is fabricated on the cleaved tip of an optical fiber, which the AFM scans in noncontact mode. The signal from the quad detector is fed to the signal in of the lock-in, and the trigger out of the laser is fed to the reference in of the lock-in. The laser is operated at 1 kHz at 50% duty cycle.

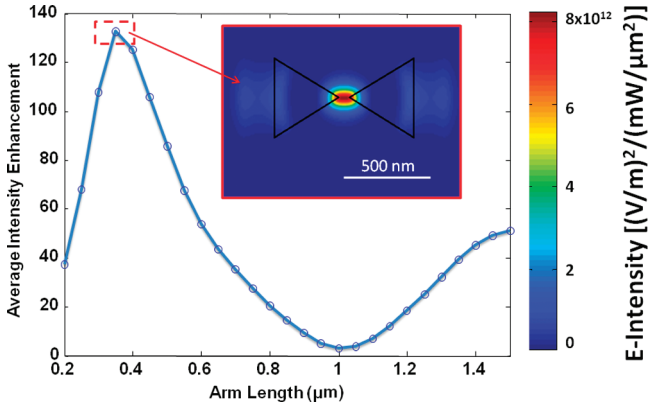

Figure 2. Simulated average intensity enhancement versus varying arm length (L) of the MDM bowtie antenna. The free space wavelength of the incident plane wave normal to the plane is considered to be 1550 nm for FDTD simulations. Different layer thicknesses of MDM were kept to be 40/30/40 nm (Au/SiO_2/Au) for all performed simulations. Electric field enhancement has been calculated in the middle of the gap at the level the of the antenna top surface using a volume monitor and normalized with the amplitude of the incident field. The gap of the antenna was fixed to be 50 nm. Simulations showed maximum resonance peak intensity at an antenna arm length of 350 nm. (Inset) FDTD simulation results showing the peak near-field intensity enhancement distribution at a level 50 nm above the top surface of the antennas (near-field region). Simulations were performed at the resonance length of the each arm (L) = 350 nm.

piconewton levels per milliwatt input power can be achieved, which is comparable to or higher than the forces achieved using a far-field optical tweezer without the bulky optics necessary for that setup.[5] Such compactness is crucial for building chip-scale biosensors.

Our primary goal is to observe the effect of the optical force on the modulation of the amplitude of the AFM tip when it is brought in this region of optical confinement. Previously, we have shown that amplitude and phase require some time (~1 ms) to respond to an external force.[21] Thus, we modulated the laser in 50% duty cycle at low frequency (1 kHz). The operating frequency of the laser was then used as the reference signal for the lock-in (see Figure 1 and Supporting Information Figure.S2 for details) We then fed the output of the lock-in back to the computer to map to the current position of the AFM, giving the optical force intensity (see Figure 4c).

The minimum force sensitivity of our AFM system, limited by thermal fluctuations,[24,25] can be calculated from $F_{min} = [(4k_BTkB)/(\omega_0 Q)]^{1/2}$, where k_B is the Boltzmann constant, T is room temperature, k is the spring constant of the cantilever (3 N/m), B is the bandwidth of measurement (set by lock-in amplifier) used in the force measurement (7.8 Hz), ω_0 is the resonant frequency of the AFM tip (~101 kHz), and Q is the quality factor of the cantilever (~160). This leads to a force sensitivity on the order of ~40 fN in our setup. Thus, measuring optical force on the order of a fraction of a piconewton is not limited by the thermal sensitivity of our system.

Our bowtie antenna is based on MDM instead of single metal design as it has shown a considerable improvement in terms of peak intensity enhancement.[19,20] To analyze the performance of our MDM bowtie antenna, we simulated the structure using three-dimensional finite-difference time-domain (FDTD) method. The nanoantenna consists of two bowtie structures separated by a gap of ~50 nm. The antenna was placed on the facet of a cleaved optical fiber. A plane wave with polarization direction along the long axis of the bowtie with wavelength of 1550 nm was used as the source for all performed FDTD simulations. During simulation, a plane wave was launched from the inside of the fiber core material at normal incidence to the surface. All material data used in the simulation is from ref 26. A detailed optimization of the bowtie was performed, similar to our previously published nanoantenna designs.[19,20] Here, we used thicknesses for the two Au and SiO_2 layers of 40 and 30 nm respectively. To find the resonant length of each arm of the bowtie, we found the average intensity enhancement at the antenna gap on the same level as the top metal surface as a function of the varying length of each arm of the bowtie (Figure 2). To achieve better accuracy, we used very fine mesh size near the antenna region. PML boundary conditions were employed across the simulation boundary and to avoid scattering effect on the results accuracy (primarily from the PML boundary layers), we put the boundary layers significantly away from the antenna region (10 times the antenna length). On the basis of our simulation, the optimum resonance length of 350 nm for one arm was chosen for the rest of the simulation and fabrication.

We then used Maxwell's stress tensor method to calculate the optical force intensity on the AFM tip. Our simulation structure consists of a MDM box (similar to fabrication) on top of a SiO_2 layer (represents the fiber material). In the box, the MDM bowtie antenna was positioned at the center with the correct sidewall angle generated during fabrication. We modeled the AFM tip as a sphere with diameter identical to the actual AFM tip (~100 nm). The position of the AFM tip was varied, and the electric field components at each position were recorded. We used a single wavelength (1550 nm) plane-wave source to model the incoming beam that comes from the optical fiber. The polarization of the plane wave was kept along the antenna axis. We placed six plane monitors surrounding the sphere to get the electric and magnetic field components at the different points of that monitor. The field components are related with Maxwell's stress tensor[12] by

dx.doi.org/10.1021/nl201780y |*Nano Lett.* 2011, 11, 3378–3382

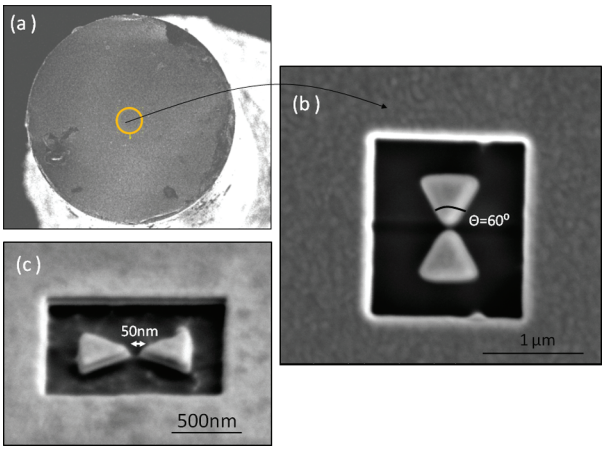

Figure 3. (a) Scanning electron microscope (SEM) image showing top-down view of the fiber before FIB milling. Schematic thick circle shows the core of the fiber. (b) Top-down view of the bowtie antenna fabricated on the core of the fiber using FIB. The darker area is the milled region where the laser core material (SiO_2) has been exposed. (c) Sideways view of the bowtie antennas showing the gap between two arms ~50 nm.

the following formula

$$T_{ij} = \varepsilon_0\varepsilon_m E_i E_j + \mu_0\mu_m H_i H_j - \frac{1}{2}\delta_{ij}(\varepsilon_0\varepsilon_m|E|^2 + \mu_0\mu_m|H|^2) \quad (1)$$

where E_i and H_i correspond to the electric and magnetic field, ε_m represents the electric permittivity, and μ_m represents the magnetic permeability for the object on which optical force is applied (AFM tip in our case). The electromagnetic force acting on the AFM tip has been calculated by the following formula

$$\langle F_i \rangle = \frac{1}{2} Re\left(\int_S T_{ij}.n_j dS\right) \quad (2)$$

where n_j is the outward normal to the surface of the six planes mentioned before.

Simulations show that the z-component of the calculated optical force is ~10 times larger than the in-plane (x- and y-) components, and this component would also have the largest effect on the amplitude of the AFM tip. Thus, for simulated force mapping (Figure 4d), we only considered the vertical component (z-) of the optical force exerted on the AFM tip. While keeping the vertical distance constant at 50 nm (near the average position of the AFM tip from the antenna top surface[21]), we simulated the z-component of the optical force at different lateral positions (x- and y-). It is important to note that the actual force is attractive, creating a trap that can be used for biosensing, but we have shown the amplitude of the force. The final simulated optical force mapping result is shown in Figure 4d.

After optimizing our design, we fabricated our devices on the end of a cleaved 125 μm Corning SMF-28E+ optical fiber. First, the fiber end was coated with Au/SiO_2/Au (40/30/40 nm) by electron-beam evaporation. The bowtie antenna was then fabricated on the surface of the coated fiber optic using focused ion beam (FIB) milling (Hellios FEI). Using the gallium ion beam at high voltage (30 keV) and a very low current (9.2 pA), a high precision milling was achieved. The fabricated antenna on the face of the fiber optic is shown in Figure 3. Figure 3c shows an oblique angle, magnified scanning electron microscope image of the bowtie antenna.

We then experimentally measured the electric field enhancement using apertureless near-field scanning optical microscopy (a-NSOM, see Supporting Information Figure.S1 for details), first developed by Hillenbrand,[27] and the optical force intensity using noncontact atomic force microscopy. Our custom-made a-NSOM setup has been previously used to characterize near-field plasmonics.[19,20] In essence, it uses a lock-in amplifier with the vibrating tip frequency as the reference and the light reflected off of the AFM tip as the signal. The output of the lock-in is then mapped to the position of the tip, simultaneously giving the user a map of the topography and near-field intensity. The AFM near-field map is shown in Figure 4e. In this way, the optical mode has been squeezed within a nanometric length scale ~150 nm that is ~10 times smaller than the operating wavelength. During its operation, the sample was illuminated at ~1 mW and the polarization of the incident beam was aligned along the long axis of the bowtie. The exact amount of coupled power to the nanoantenna was certainly lower than the laser power due to different coupling losses. Thus, it is difficult to quantify the exact amount of power confined in the "hot spot," as done in aperture-NSOM.[28]

Figure 4c,d shows both the experiment and simulation of the optical force map, respectively. Both show a central spot on the order of 0.5 pN (see Supporting Information for details) and lobes at the ends of the bowtie arms where the force is diminished compared to the central spot, showing good agreement. The central spot of the experimental image is likely larger compared to the simulation because in the simulation we considered the AFM tip as a sphere instead of using its actual pyramidal structure. The optical force was only observed in the bowtie whose long axis was aligned with the incident electric field (Figure 4c). In the lower bowtie, where the polarization was perpendicular to the long axis, no optical force was observed. The spatial resolution of this technique is limited by two factors, first, the radius of curvature of the AFM tip used for the scan, and second, the bandwidth of the lock-in amplifier used in the experimental setup. For the radius of curvature of the AFM tip, there is a trade-off: the smaller the radius, the greater resolution, but also smaller interaction with the optical force generated by the nanoantenna, which is why we prefer a tip with a radius of about 100 nm. There is also a trade-off with bandwidth of the lock-in: the greater the bandwidth of the lock-in, the smaller the spot size of the scan will be, but also the noise will be higher. Note that the long-term mechanical stability of the sample determines a lower bound on the scan speed, which determines a minimum bandwidth one can choose.

In conclusion, we have presented a method for mapping the optical force intensity created by a plasmonic nanoantenna in noncontact mode with an atomic force microscope. We have used 3D FDTD simulations to optimize the design of the MDM bowtie antenna resonant at an operating wavelength of 1550 nm. Optical force was calculated using Maxwell's stress tensor method. After the design process, the antenna was fabricated on the face of the MDM-coated optical fiber using focused ion beam milling. We used a homemade apertureless near-field scanning optical microscope to simultaneously measure the topography and near-field intensity of the antenna. Finally, we presented a method to map the optical force generated on an AFM tip due to the optical confinement. We believe that this work has many applications in areas ranging from

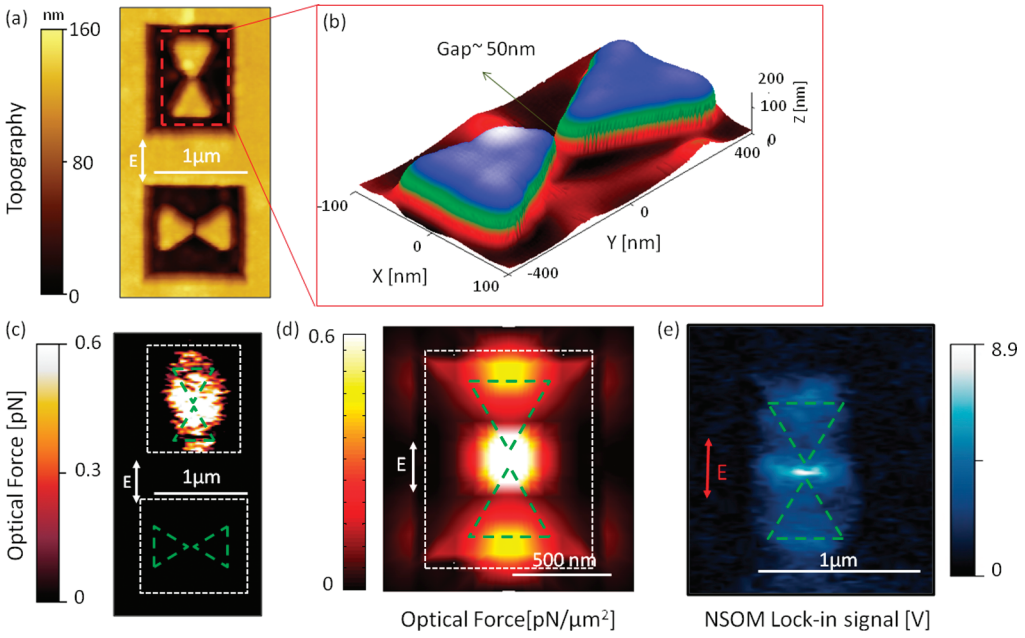

Figure 4. (a) Topographical image showing two bowtie antennas where the E-field was aligned along the long axis for the top antenna. Due to FIB milling, a box was created around each antenna. (b) A 3D view of the topographical image of the top antenna shown in (a). Thickness from the top of the antenna to the core material is ~160 nm, which is a higher than the designed MDM thickness (110 nm) value because of overmilling of the fiber core material. (c) Measured optical force map of the bowtie antenna. Resonant top antenna shows a force map with a central spot near the antenna gap and two side lobes at the end of the fanlike segment. This matches well with the simulated optical force intensity map shown in (d). The simulations have been performed on identical antenna structure with the box. Green dashed lines in (c−e) demarcate the antenna structure while the white dashed line in (c) and (d) demarcates the box. (e) Apertureless near-field scanning optical microscope (a-NSOM) image of MDM bowtie antenna. The antenna was designed to be resonant at a wavelength of 1550 nm and incident electric field was aligned along the long axis of the antenna.

optical trapping in biosensing[16,17,29] to optical switching in telecommunication.[30]

■ ASSOCIATED CONTENT

Supporting Information. Additonal information and figures. This material is available free of charge via the Internet at http://pubs.acs.org.

■ AUTHOR INFORMATION

Corresponding Author

*E-mail: hmohseni@ece.northwestern.edu.

■ REFERENCES

(1) Kippenberg, T. J.; Vahala, K. J. *Science* **2008**, *321* (5893), 1172–1176.
(2) Tsu, T. C. *Ars J.* **1959**, *29* (6), 422–427.
(3) Metzger, C. H.; Karrai, K. *Nature* **2004**, *432* (7020), 1002–1005.
(4) Arcizet, O.; Cohadon, P. F.; Briant, T.; Pinard, M.; Heidmann, A. *Nature* **2006**, *444* (7115), 71–74.
(5) Knoner, G.; Ratnapala, A.; Nieminen, T. A.; Vale, C. J.; Heckenberg, N. R.; Rubinsztein-Dunlop, H. *Lab Chip* **2006**, *6* (12), 1545–1547.
(6) Ashkin, A.; Dziedzic, J. M.; Yamane, T. *Nature* **1987**, *330* (6150), 769–771.
(7) Gahagan, K. T.; Swartzlander, G. A. *Opt. Lett.* **1996**, *21* (11), 827–829.
(8) Neuman, K. C.; Block, S. M. *Rev. Sci. Instrum.* **2004**, *75* (9), 2787–2809.
(9) Volpe, G.; Quidant, R.; Badenes, G.; Petrov, D. *Phys. Rev. Lett.* **2006**, *96*, 23.
(10) Xu, H.; Käll, M. *Phys. Rev. Lett.* **2002**, *89* (24), 246802.
(11) Cetin, A. E.; Yanik, A. A.; Yilmaz, C.; Somu, S.; Busnaina, A.; Altug, H. *Appl. Phys. Lett.* **2011**, *98*, 11.
(12) Ploschner, M.; Mazilu, M.; Krauss, T. F.; Dholakia, K. *J. Nanophotonics* **2010**, 4.
(13) Righini, M.; Zelenina, A. S.; Girard, C.; Quidant, R. *Nat. Phys.* **2007**, *3* (7), 477–480.
(14) Juan, M. L.; Gordon, R.; Pang, Y. J.; Eftekhari, F.; Quidant, R. *Nat. Phys.* **2009**, *5* (12), 915–919.
(15) Yang, X.; Liu, Y.; Oulton, R. F.; Yin, X.; Zhang, X. *Nano Lett.* **2011**, *11* (2), 321–328.
(16) Huang, L.; Maerkl, S. J.; Martin, O. J. F. *Opt. Express* **2009**, *17* (8), 6018–6024.
(17) Righini, M.; Ghenuche, P.; Cherukulappurath, S.; Myroshnychenko, V.; de Abajo, F. J. G.; Quidant, R. *Nano Lett.* **2009**, *9* (10), 3387–3391.
(18) Gelfand, R. M.; Bruderer, L.; Mohseni, H. *Opt. Lett.* **2009**, *34* (7), 1087–1089.
(19) Dey, D.; Kohoutek, J.; Gelfand, R. M.; Bonakdar, A.; Mohseni, H. *Opt. Lett.* **2010**, *35* (16), 2783–2785.
(20) Dey, D.; Kohoutek, J.; Gelfand, R. M.; Bonakdar, A.; Mohseni, H. *IEEE Photonics Technol. Lett.* **2010**, *22* (21), 1580–1582.
(21) Kohoutek, J.; Wan, I. Y. L.; Mohseni, H. *Appl. Phys. Lett.* **2010**, *96* (6), 063106.
(22) Yu, N. F.; Cubukcu, E.; Diehl, L.; Bour, D.; Corzine, S.; Zhu, J. T.; Hofler, G.; Crozier, K. B.; Capasso, F. *Opt. Express* **2007**, *15* (20), 13272–13281.
(23) Griffiths, D. J. *Introduction to Electrodynamics*, 3rd ed.; Prentice-Hall: Upper Saddle River, NJ, 1999.
(24) Kohoutek, J.; Wan, I. Y. L.; Memis, O. G.; Mohseni, H. *Opt. Express* **2009**, *17* (17), 14458–14465.
(25) Li, M.; Tang, H. X.; Roukes, M. L. *Nat. Nanotechnol.* **2007**, *2* (2), 114–120.
(26) Palik, D. *Handbook of Optical Constants of Solids*; Academic: New York, 1985; Vol. 1.

(27) Hillenbrand, R.; Knoll, B.; Keilmann, F. *J. Microsc. (Oxford, U.K.)* **2001**, *202*, 77–83.
(28) Hecht, B.; Sick, B.; Wild, U. P.; Deckert, V.; Zenobi, R.; Martin, O. J. F.; Pohl, D. W. *J. Chem. Phys.* **2000**, *112* (18), 7761–7774.
(29) Gelfand, R. M.; Dey, D.; Kohoutek, J.; Bonakdar, A.; Hur, S. C.; Carlo, D. D.; Mohseni, H. *Opt. Photonics News* **2011**, *22* (32), 32–37.
(30) Wang, Z. F.; Cao, W.; Shan, X. C.; Xu, J. F.; Lim, S. P.; Noell, W.; de Rooij, N. F. *Sens. Actuators, A* **2004**, *114* (1), 80–87.